Korean J. Chem. Eng., **28**(11), 2163-2169 (2011)
DOI: 10.1007/s11814-011-0101-x

Phase behavior analysis of heavy oil containing asphaltene

Hanam Son*, Youngsoo Lee, Junwoo Seo***, Sangjin Kim***, Wonsuk Lee*, and Wonmo Sung***,†**

*Korea Institute of Geoscience and Mineral Resources, Daejeon 305-350, Korea
**R&D Division, Korea Gas Corporation, Ansan 426-790, Korea
***Department of Natural Resources and Environmental Engineering, Hanyang University, Seoul 133-791, Korea
(*Received 15 March 2011 • accepted 13 April 2011*)

Abstract−A thermodynamic asphaltene precipitation model was developed based on the model of Nghiem et al. using the Peng-Robinson equation of state (PR EOS). This model calculates the amount of asphaltene precipitation based on changes in temperature and pressure. The effects of asphaltene precipitation on rock properties were investigated by observing changes in porosity and permeability. In this model, phase equilibrium was achieved by repeatedly reducing the amount of the asphaltene component, in contrast to the model of Qin et al. using the secant method. The results of this model were compared with experimental data of measured precipitation, based on changes in pressure, and agreed more closely than the model of Qin et al. Our results also confirmed that the maximum precipitation of asphaltene occurred at the bubble-point pressure. Thus, using the model, we verified that the precipitation pattern of asphaltene depended on temperature and pressure, and it is expected that changing patterns in reservoir productivity can be analyzed using asphaltene precipitation in heavy oil-containing asphaltene.

Key words: Asphaltene Precipitation, Porosity Changes, Permeability Changes, Heavy Oil, PR EOS

INTRODUCTION

Asphaltene exists in the oil phase of heavy oil under the initial conditions of a reservoir [1], but can be solid phase due to changes in temperature and pressure. If asphaltene precipitates in a reservoir, reservoir productivity can decrease due to reduced porosity and permeability. Asphaltene can also plug a pipeline. Problems related to asphaltene precipitation have been reported in Venezuela [2], Algeria [3], California [4], Kuwait [5], and other locations. Mechanical and chemical cleaning methods of wellbores are continuously improved to maintain production; however, facilities and money are required for the costs associated with asphaltene treatment.

The need to predict asphaltene precipitation to minimize damage during oil production has been recognized, and many models have been developed since the 1980s. Hirschberg et al. [6] proposed a solubility model that was based on the Soave-Redlich-Kwong equation of state (SRK EOS) and Flory-Huggins theory, in which asphaltene stability was described in terms of reversible solution equilibrium. Leontaritis and Mansoori [7] developed a model based on statistical thermodynamics and colloid engineering. Thomas et al. [8] proposed a solid model that assumed that asphaltene is a single component having the largest molecular weight in the oil. Nghiem et al. [9] proposed a model that considered the precipitated asphaltene as a pure dense phase, while the heaviest component in the oil could be split into two parts: non-precipitating and precipitating components. The precipitating component was determined to be asphaltene. The amount of asphaltene precipitation can be calculated by equating the fugacities of asphaltene component in the liquid and solid phases.

†To whom correspondence should be addressed.
E-mail: wmsung@hanyang.ac.kr

In this study, the equilibrium of fugacities between the liquid and solid phases was derived using the equal-difference method to increase the numerical accuracy, based on the model of Nghiem et al. [9]. Those results were compared with Qin's model [10], which used the secant method for calculating the equilibrium of fugacities between the liquid and solid phases for the experimental data of Burke et al. [11]. In this study, the amount of asphaltene precipitation, based on variation in pressure and temperature, was calculated, and the effects of asphaltene precipitation on rock properties were investigated. Porosity and permeability changes are also presented.

ASPHALTENE PRECIPITATION MODEL

Asphaltenes are heavy hydrocarbon molecules that are dissolved in aromatic series, such as benzene but are not soluble in paraffin, which has a lower molecular weight. Asphaltene combines with resin in a stable colloidal state and is dispersed in crude oil, but can precipitate when temperature, pressure, and composition change [12]. As temperature increases, resin is desorbed from the asphaltene surface, and asphaltene particles agglomerate, increasing the amount of precipitation (Fig. 1). However, if the temperature rises continuously, the amount of precipitation will decrease as the solubility of asphaltene in the oil increases. Thus, there is a temperature at which the maximum amount of asphaltene precipitation occurs. Asphaltene precipitation due to pressure changes is related to solubility, which varies based on the bubble-point pressure. When the pressure is above the bubble point, the amount of precipitation will increase until the pressure reaches the bubble point. If the pressure decreases below the bubble point, the amount of precipitation will decrease [6].

In this model, asphaltene is assumed to be a single component having the largest molecular weight in the hydrocarbon and is split

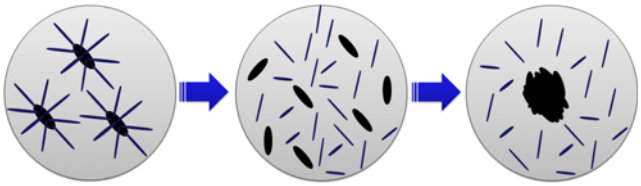

Fig. 1. Mechanism of asphaltene precipitation due to increasing temperature.

into precipitating and non-precipitating components. Fugacity in the gas-liquid phase was computed via flash calculations using the Peng-Robinson equation of state (PR EOS), and the fugacity of the solid phase was calculated using the fugacity equation of asphaltene in the solid phase used by Nghiem et al. [9]. The PR EOS predicts the density of liquids and other fluid properties in the vicinity of the critical region more accurately than the SRK EOS.

The expression of the PR EOS is

$$p=\frac{RT}{V-b}-\frac{a}{V(V+b)+V(V-b)} \tag{1}$$

If Eq. (1) is expressed as a function of the compressibility factor (Z-factor) on the liquid and vapor phases, it is arranged into a cubic equation:

$$Z^3-(1-B)Z^2+(A-3B^2-2B)Z-(AB-B^2-B^3)=0 \tag{2}$$

where the dimensionless parameters A and B are defined as

$$A=\frac{aP}{R^2T^2} \tag{3}$$

$$B=\frac{bP}{RT} \tag{4}$$

Here, T and P are the setting temperature and the pressure of the system, respectively, R is the ideal gas constant, and a and b are parameters defined as

$$a=\sum_{i}^{n_c}\sum_{j}^{n_c}x_i x_j(1-k_{ij})\sqrt{a_i a_j \alpha_i \alpha_j} \tag{5}$$

$$b=\sum_{i}^{n_c}x_i b_i \tag{6}$$

where k_{ij} is the binary interaction parameter of each component, and a_i, b_i, and α_i can be calculated based on critical temperatures, critical pressures, and the acentric factors of each component.

$$a_i=0.45724\frac{R^2T_{ci}^2}{P_{ci}} \tag{7}$$

$$b_i=0.07780\frac{RT_{ci}}{P_{ci}} \tag{8}$$

$$\alpha_i=[1+(0.37464+1.54226\omega_i-0.26992\omega_i^2)(1-\sqrt{T_{ri}})]^2 \tag{9}$$

The compressibility factor of the liquid and vapor phases can be solved using Eqs. (2)-(9), and the fugacity and saturation pressure can be obtained. However, because the composition and the compressibility factor of the liquid and vapor phases near the critical point have the same value, it is difficult to calculate the saturation pressure using the PR EOS [13]. To calculate the saturation pressure near the critical point, a new scheme is proposed in this study.

To generate the phase envelope near the critical point, the saturation pressure was calculated by flash calculations, and the point that did not converge in the bubble-point line was assumed to be a critical point. Then, the dew points from the critical point were calculated using the slope of the dew points, which are the ratios of the slope of each dew-point pressure (①-②, ②-③, ..., ⑥-⑦) to the total slope between the starting point of the dew-point pressure (①) and the point that did not converge (⑦), as seen in Fig. 2. This method assumes that the slopes of the dew points near the critical region are similar to the slopes of the dew-point pressures at the starting area but have opposite directions. Using this method, total dew-

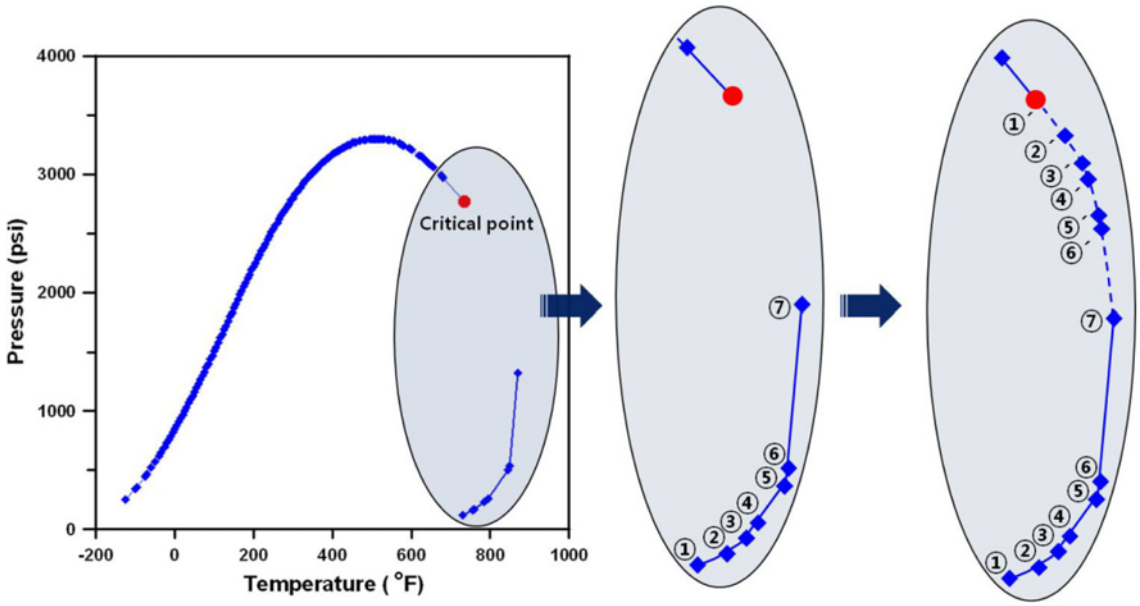

Fig. 2. Schematic diagram for calculating saturation pressure in the critical region.

Table 1. Composition of light and heavy oil

Component	Composition (%)	
	Light oil	Heavy oil
CO_2	-	5
N_2	-	5
C_1	70	10
C_2	10	10
C_3	10	-
iC_4	5	-
nC_4	5	-
C_{7+}	-	70

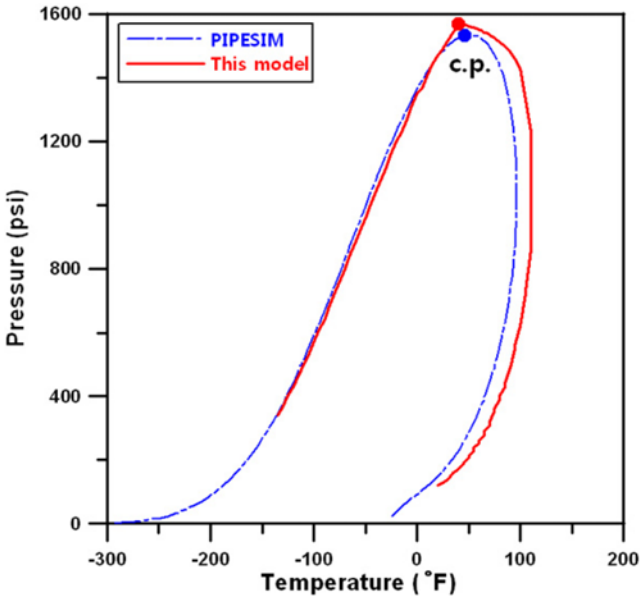

Fig. 3. Comparison of the phase envelope for light oil.

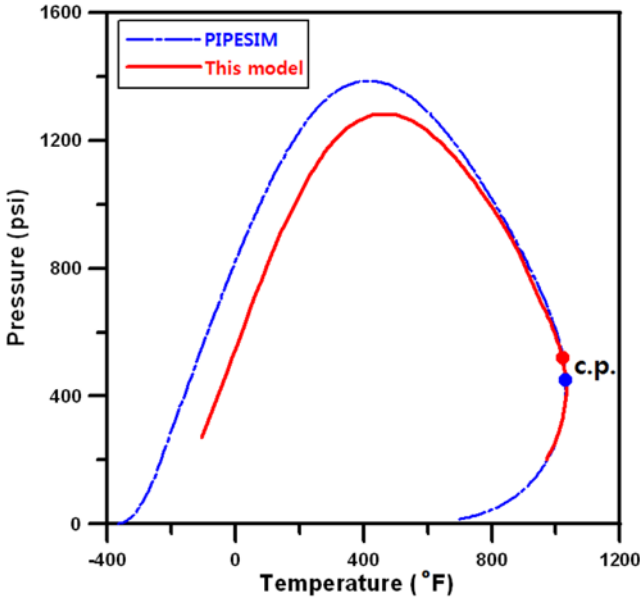

Fig. 4. Comparison of the phase envelope for heavy oil.

point pressures were calculated up to the critical point. The projected phase envelope was compared with steady-state multiphase flow simulation software (PIPESIM, Schlumberger) for light- and heavy-component oils in Table 1 and Figs. 3 and 4, respectively. Overall, this model agreed with the commercial model.

The asphaltene precipitation model was developed for isothermal and thermal processes. For isothermal processes, the equation of asphaltene fugacity from Nghiem et al. [9] was used for the solid phase to predict the amount of asphaltene precipitation. This phase is referred to as the asphalt phase.

$$\ln f_a = \ln f_a^* + \frac{V_a(P - P^*)}{RT} \tag{10}$$

where f_a and f_a^* are the fugacities of pure asphaltene at pressures p and p^*, respectively, and V_a is the molar volume of asphaltene. In a mixture of n_c components, asphaltene is the n_c^{th} component. When the vapor, liquid, and solid phases coexist, the following thermodynamic equilibrium equations are satisfied.

$$\ln f_{iv} = \ln f_{il} \qquad i = 1, \ldots, n_c - 1 \tag{11}$$

$$\ln f_{n_c v} = \ln f_{n_c l} = \ln f_a \tag{12}$$

In Eqs. (11) and (12), the fugacity of the liquid and vapor phases can be calculated from cubic EOS. The presence of a solid phase satisfies the following criterion:

$$\ln f_{n_c l} \geq \ln f_a \tag{13}$$

When a solid phase exists, the amount of asphaltene precipitation can be obtained using the following equilibrium condition:

$$\ln f_{n_c l} = \ln f_a \tag{14}$$

Qin et al. [10] adjusted the composition of the asphaltene component to satisfy the conditions of Eq. (14) using the secant method; however, in this model, to increase accuracy, the phase equilibrium was achieved by repeatedly reducing the mole fraction of the n_c component and by increasing the mole fraction of the remaining components. The flowchart for the algorithm is shown in Fig. 2.

In the thermal process, the equation of asphaltene fugacity in the thermal process by Kohse et al. [14] was used. The calculation process is the same as the isothermal process. However, Eq. (10) was used by substituting the following formula:

$$\ln f_a = \ln f_a^* + \frac{V_a}{R}\left[\frac{P - P_{tp}}{T} - \frac{P^* - P_{tp}}{T^*}\right] - \frac{\Delta H_{tp}}{R}\left[\frac{1}{T} - \frac{1}{T^*}\right] - \frac{\Delta C_p}{R}\left[\ln\left(\frac{T^*}{T}\right) - T_{tp}\left(\frac{1}{T} - \frac{1}{T^*}\right)\right] \tag{15}$$

where P_{tp}, T_{tp} are pressure and temperature at the triple point, respectively, and ΔC_p, ΔH_{tp} are the heat capacity difference between the liquid and solid phases and the enthalpy of fusion at the triple point, respectively.

1. Model Validation and Application

The amount of asphaltene precipitation at various pressures was calculated for the sample in Table 2 from Qin et al. [10]. Fig. 6 compares the results from the asphaltene precipitation model implemented in this study with those from the model of Qin et al. [10] using the experimental data of Burke et al. [11]. Compared with the previous model and the experimental data, our model predicts the precipita-

Table 2. Oil sample data for asphaltene precipitation [9]

Component	Composition (%)	Molecular weight (g/mol)
CO_2	2.46	44.01
C_1-C_2	40.41	17.42
C_3-C_5	7.55	53.52
C_6-C_{19}	27.19	164.22
C_{20}-C_{30}	10.64	340.93
C_{31+}	11.75	665.62

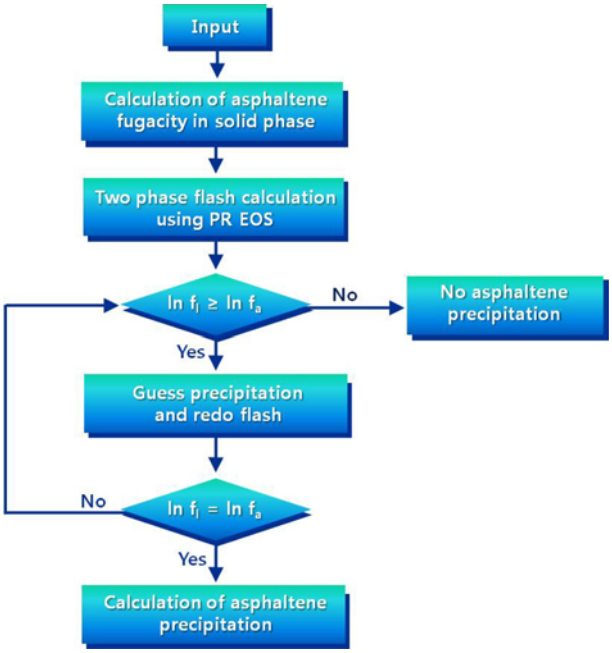

Fig. 5. Flowchart of the asphaltene precipitation model.

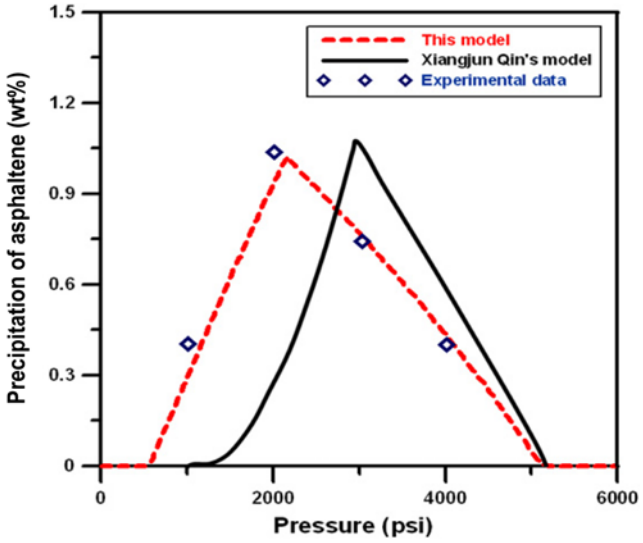

Fig. 6. Comparison of simulation results and experimental data for asphaltene precipitation.

tion more accurately.

The amount of asphaltene precipitation increased with decreasing pressure until the bubble-point pressure. Below the bubble-point

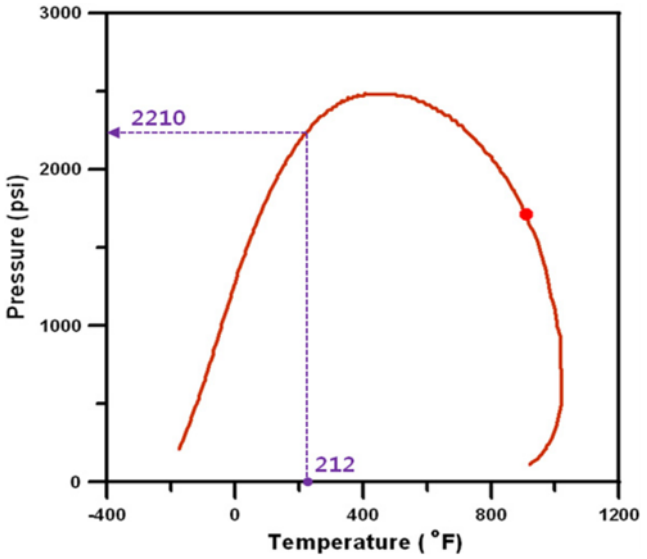

Fig. 7. Phase envelope generated by this model for Table 2.

pressure, the amount of precipitation was reduced by the release of dissolved gases [6]. Additionally, when temperature increased, the resin desorbed from the asphaltene surface, and asphaltene particles agglomerated, increasing the amount of precipitation. The amount of asphaltene precipitation, based on pressure and temperature, was predicted and analyzed.

Fig. 7 shows the phase envelope generated by this model from composition data (Table 2) proposed by Burke et al. [11] at 212 °F. According to the phase-envelope curve, the bubble-point pressure at 212 °F was 2,210 psi. Additionally, asphaltene began to precipitate at 5,170 psi, and pressure decreased to 2,200 psi at the maximum precipitation of 1.04 wt%; asphaltene disappeared at 520 psi and 212 °F (Fig. 8(a)). These results indicate that the maximum amount of asphaltene precipitation occurred at the bubble-point pressure, and this model predicted the amount of asphaltene precipitation at a reasonable level. Next, asphaltene precipitation was predicted based on changes in temperature. As the temperature increased above 210 °F, the amount of asphaltene precipitation increased, reaching a maximum at 240 °F. However, above 240 °F, the amount of precipitation decreased (Fig. 8(b)). Thus, this fluid has a minimum solubility for asphaltene at 240 °F, regardless of pressure variation. Fig. 9 shows the maximum amount of precipitation as a function of temperature. Based on these results, we can predict the maximum amount of precipitation with respect to temperature variation in situations such as thermal flooding and injection. Our results also confirm that maximum asphaltene precipitation occurs at the bubble-point pressure, regardless of temperature variation (Fig. 10).

The effects of asphaltene precipitation on rock properties are due to porosity and permeability changes. Because asphaltene precipitates as solid grains that are adsorbed onto rock surfaces, it plugs the formation pores and becomes immobile in the reservoir [10]. Changes in porosity and permeability due to asphaltene precipitation can be expressed as

$$\phi_a = \phi^* \left(1 - \frac{\hat{V}_a}{\phi^* V_b}\right) \tag{16}$$

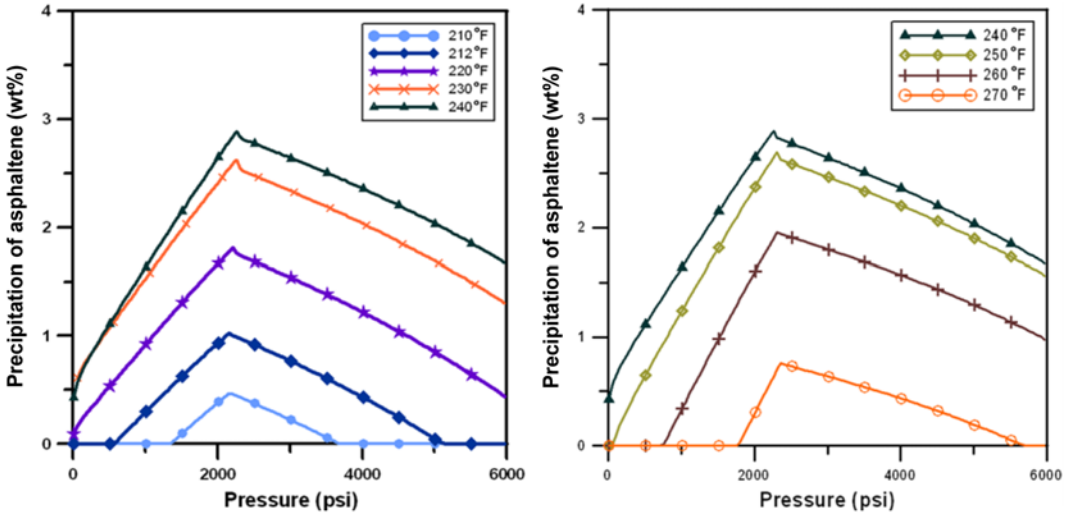

Fig. 8. Asphaltene precipitation as a function of temperature: (a) increasing precipitation with increasing temperature and (b) decreasing precipitation with increasing temperature.

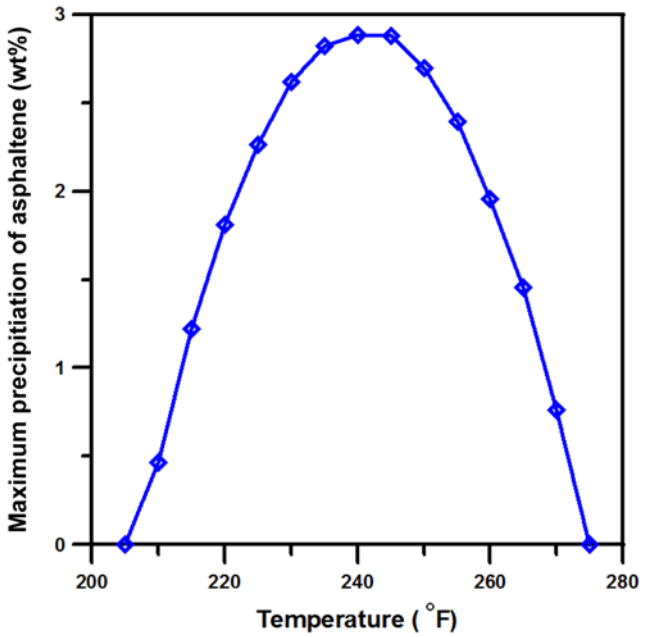

Fig. 9. Maximum amount of asphaltene precipitation as a function of temperature.

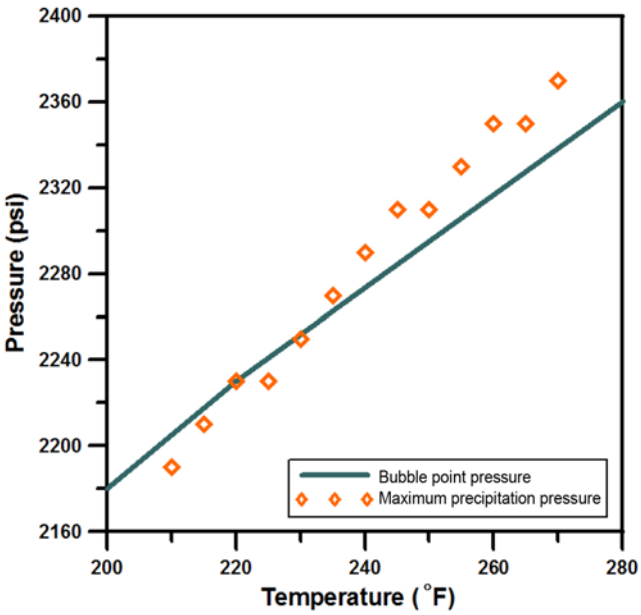

Fig. 10. Comparison of bubble-point pressure and maximum precipitation pressure.

$$k=u\phi^{v} \quad (17)$$

where ϕ^{*} is the porosity without asphaltene precipitation.

It is assumed that a sandstone reservoir has a porosity of 0.2 without asphaltene precipitation. Points u and v are from rock classification data in Table 3 [15]. Fig. 11 shows that the porosity decreased to 1.05%, and permeability decreased to 5.33% at 2,200 psi, which is the maximum point of asphaltene precipitation. Porosity and permeability were 0.2 and 37.95 md, respectively, at 200 °F (no asphaltene precipitation). As temperature increased to 240 °F (maximum asphaltene precipitation), porosity and permeability decreased to 2.94% and 14.3%, respectively (Fig. 12). Many researchers have concluded that rock permeability is more significantly affected than rock porosity by the precipitation process [16,17]. However, no general relationship between precipitation and permeability has been identified from previous experiments. Thus, this procedure is useful for predicting the effects of asphaltene precipitation on porosity and permeability.

Table 3. Constants u and v for different rock-fabric classifications [14]

Classification	Constant u	Constant v
1	45.35×10^{8}	8.637
2	1.595×10^{5}	5.184
3	2.884×10^{3}	4.276

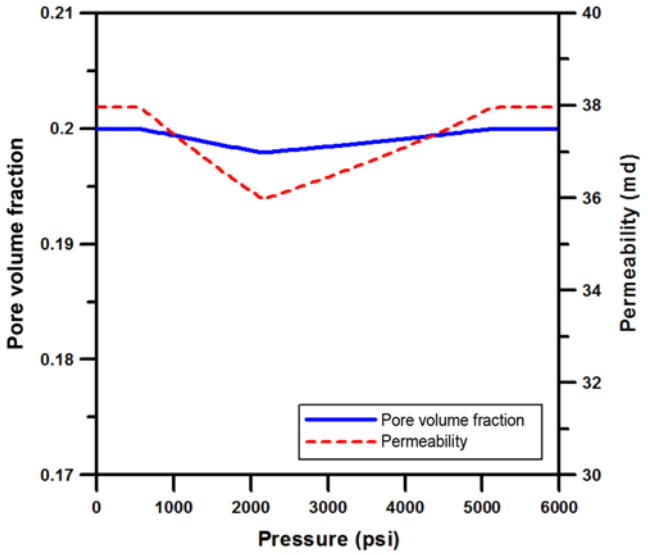

Fig. 11. Change in pore volume fraction and permeability due to asphaltene precipitation as a function of pressure (212 °F).

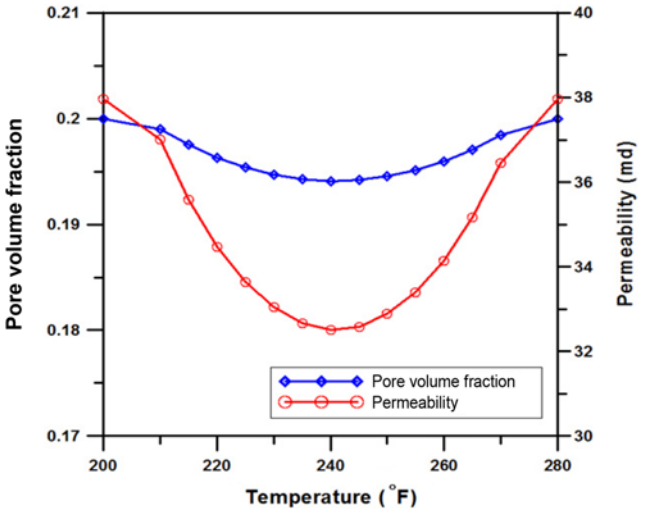

Fig. 12. Change of pore volume fraction and permeability due to asphaltene precipitation as a function of temperature (2,280 psi).

CONCLUSIONS

We developed a thermodynamic asphaltene precipitation model. The fugacities of the liquid and solid phases were calculated using a flash calculation, and the fugacity for the solid phase was computed using the fugacity equation of asphaltene in the solid phase, derived by Ngheim et al. The amount of asphaltene precipitation at various pressures and temperatures was calculated, and the effects of asphaltene precipitation on rock properties were investigated based on porosity and permeability.

The saturation pressure calculated by this model was compared with calculations using commercial software for light and heavy oils. The results of this model were in good agreement with those of the commercial model.

Compared with the model of Qin et al. and the experimental data of Burke et al. for predictions of asphaltene precipitation with pressure variation, this model predicted the precipitation more accurately.

Using this model, we can predict the maximum amount of precipitation at various temperatures for situations, such as thermal flooding and steam injection. Our study also confirms that the maximum precipitation of asphaltene occurs at the bubble-point pressure, regardless of temperature and pressure variation.

Asphaltene precipitation affected the porosity and permeability of rocks. Thus, the proposed methods are useful for predicting the effects of asphaltene precipitation on porosity and permeability.

ACKNOWLEDGEMENTS

This work was supported by the Energy Efficiency & Resources of the Korean Institute of Energy Technology Evaluation and Planning (KETEP) grant, funded by the Korean Government Ministry of the Knowledge Economy (No. 2010RER11P030000).

NOMENCLATURE

Z : compressibility factor
R : gas constant
T : temperature
P : pressure
V : volume
A, B : dimensionless parameter for calculation of compressibility factor
a, b : parameter for calculation of A, B
x_i, x_j : composition of component i, j
a_i, a_j : parameter for calculation of a, b
α_i, α_j : parameter for calculation of a, b
k_{ij} : interaction coefficient between component i and j
ω_i : acentric factor of component i
T_{ci} : critical temperature of component i
P_{ci} : critical pressure of component i
f_a : fugacity of pure asphaltene at pressures p
f_a^* : fugacity of pure asphaltene at pressures p^*
f_{ij} : fugacity of component i in phase j
p^* : reference pressure
V_a : molar volume of asphaltene
P_{tp} : triple-point pressure
T_{tp} : triple-point temperature
ΔH_{tp} : enthalpy of fusion at triple-point
ΔC_p : heat capacity difference ($C_{pl} - C_{ps}$)
u, v : coefficient for rock-fabric classifications
ϕ : porosity
ϕ^* : porosity without asphaltene precipitation
ϕ_a : porosity by asphaltene precipitation
K : permeability
$\hat{V}_a$: precipitated asphaltene volume
V_b : bulk volume

REFERENCES

1. S. H. Yoon, S. D. Bhatt, W. K. Lee, S. Y. Jeong, J. O. Baeg and C. W. Lee, *Korean J. Chem. Eng.*, **26**, 64 (2009).

2. M. C. Garcia, M. Henriquez and J. Orta, the SPE International Symposium on Oil Field Chemistry, Houston, U.S.A. (2003).
3. C. E. Haskett and M. Tatera, *J. Pet. Technol.*, **17**, 387 (1965).
4. R. N. Tuttle, *J. Pet. Technol.*, **35**, 1192 (1983).
5. C. S. Kabir and A. K. M. Jamaluddin, *SPEPF*, **17**, 251 (2002).
6. A. Hirschberg, L. N. J. de Jong and J. G. Meijer, *SPE*, **24**, 283 (1984).
7. K. J. Leontaritis and G. A. Mansoori, the SPE International Symposium on Oil Field Chemistry, San Antonio, U.S.A. (1987).
8. F. B. Thomas, D. B. Bennion and D. W. Bennion, *J. Pet. Technol.*, **31**, 22 (1992).
9. L. X. Nghiem, M. S. Hawtm and R. Nutakki, the SPE Annual Technical Conference and Exhibition, Houston, U.S.A. (1993).
10. X. Qin, W. Peng, S. Kamy and G. A. Pope, *Ind. Eng. Chem. Res.*, **39**, 2644 (2000).
11. N. E. Burke, R. E. Hobbs and S. F. Kashou, *J. Pet. Technol.*, **42**, 1440 (1990).
12. M. Li, P. Guo and S. Li, the SPE Permian Basin Oil and Gas Recovery Conference, Midland, U.S.A. (2001).
13. D. X. Young, *J. Canadian Pet. Technol*, **39**, 35 (2000).
14. B. F. Kohse, L. X. Nghiem, H. Maeda and K. Ohno, the SPE Asia Pacific Oil and Gas Conference and Exhibition, Brisbane, Australia (2000).
15. F. J. Lucia, *AAPG Bulletin*, **79**, 896 (1995).
16. T. M. de Pedroza, G. Calderon and A. Rico, *SPE Advanced Technology Series*, **4**, 185 (1996).
17. A. de Danesh, E. Krinis and G. Henderson, *Peden, J. Chem. Eng. Res. Des.*, **66**, 339 (1988).